

Origin of the very high energy gamma-ray emission from pulsar wind nebulae

Gwenael Giacinti,^{a,b,*} Brian Reville^a and John G. Kirk^a

^aMax-Planck-Institut für Kernphysik,
Postfach 103980, 69029 Heidelberg, Germany

^bTsung-Dao Lee Institute, Shanghai Jiao Tong University,
800 Dongchuan Road, Minhang District, Shanghai 200240, China
E-mail: Gwenael.Giacinti@mpi-hd.mpg.de

We study electron and positron acceleration at the termination shock of a striped pulsar wind by integrating particle trajectories in a prescribed model of the magnetic field and flow pattern. We find that drift motion on the shock surface maintains either electrons or positrons on Speiser orbits in a ring-shaped region close to the equatorial plane of the pulsar, where they are accelerated to very high energy by the first-order Fermi mechanism. We calculate the resulting inverse Compton emission from these electrons, and demonstrate that the observed $> \text{TeV}$ gamma-ray emission from the Crab Nebula can be well reproduced for reasonable parameters of the Crab pulsar wind and turbulence levels in the nebula. We show that future observations of the Crab Nebula at $\sim \text{PeV}$ energies, e.g. by LHAASO, will allow for putting relevant constraints on parameters of the Crab pulsar wind that are still poorly known.

37th International Cosmic Ray Conference (ICRC 2021)
July 12th – 23rd, 2021
Online – Berlin, Germany

*Presenter

1. Introduction

The Crab Nebula is thought to accelerate electrons and/or positrons up to at least a PeV [1]. However, the mechanisms and sites of particle acceleration remain uncertain. The photon index of the Nebula in X-rays [2] is very close to expectations for electrons accelerated by the first order Fermi mechanism at an ultra-relativistic shock with isotropic particle scattering [3, 4]. However, the magnetic field is expected to be toroidal close to the pulsar wind termination shock (TS), i.e., the TS is perpendicular. On the one hand, diffusive shock acceleration is known to be inoperative at perpendicular shocks [5, 6]. On the other hand, the toroidal field in the downstream region of the TS is expected to change sign across the equatorial plane of the pulsar [7]: in this region, turbulence levels may be higher, and diffusive shock acceleration might still operate. We study here electron and positron acceleration in this region of the TS, by propagating individual particles in a model of the magnetic field and flow pattern [8], and we calculate the resulting emission in X-rays (from synchrotron) and in gamma-rays (from inverse Compton).

2. Model

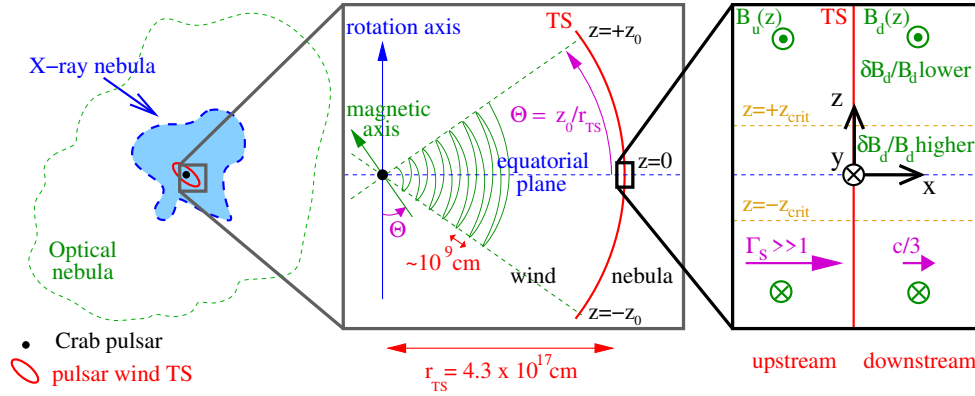


Figure 1: Sketch of the Crab Nebula (left panel), with the location and characteristics of the region studied in this work (right panel). A description of this Figure is provided in the text below.

Fig. 1 shows a sketch of the region of interest in the Crab Nebula. In the left panel, the X-ray and optical nebulae are drawn as they appear on the sky, together with an estimate of the position of the TS. The centre panel is an enlargement of the equatorial region of the Crab pulsar wind (labelled “wind”). The TS is drawn as a solid red arc of radius $r_{TS} \approx 4.3 \times 10^{17}$ cm. The rotation axis of the pulsar (blue arrow) lies in the plane of the figure, and the magnetic axis (green arrow) is drawn at a phase at which it lies in this plane too. The horizontal dashed blue line corresponds to the equatorial plane. Magnetic field oscillations, or stripes, are present upstream of the TS between the latitudes $\pm\Theta$, where Θ is the angle between the magnetic and rotation axes. Upstream, the magnetic field is toroidal and changes sign across the current sheet (thin green line). The stripes are destroyed at (or before) the TS, leaving a net toroidal component in the downstream “nebula”, which reverses across the equatorial plane, and has an amplitude that grows with distance from this plane [7]. The black rectangle in the centre panel, and its enlargement in the right panel correspond to the region

we model. It is typically a few percent of the shock area, so we take the TS to be plane and the flow planar. In the cartesian coordinate system defined in Fig. 1, the fluid flows along $+\hat{\mathbf{x}}$. In the simulations, we set the Lorentz factor of the fluid in the upstream ($x < 0$) to $\Gamma_s = 100$, but the results do not depend on this choice, provided $\Gamma_s \gg 10$. Downstream, the fluid velocity is assumed to be $c/3$, and the residual toroidal field, defined in the downstream rest frame (DF), is modelled as $\mathbf{B}_d(z) = -B_{d,0}(z/z_0)\hat{\mathbf{y}}$ — with $z_0 = \Theta r_{\text{TS}}$ and $B_{d,0} = +1\text{mG}$. The polarity of the pulsar is set by the sign of $B_{d,0}$. Upstream, the wavelength of the stripes ($\approx 10^9$ cm) is much smaller than the gyroradii of the particles we considered, which, therefore, probe only the phase-averaged field (for deflections), given by the jump conditions to be $\mathbf{B}'_u(z) = (-B_{d,0}/(2\sqrt{2}\beta_s)) \times (z/z_0)\hat{\mathbf{y}}$, in the shock rest frame, where β_s is the velocity of the upstream fluid in this frame. Because the downstream flow is subsonic, turbulence is able to fill the entire Nebula external to the TS. Therefore, on top of the residual toroidal field, we add, in this region, a homogeneous 3D turbulent component, with root-mean-square strength δB_d — defined in the DF. Thus, the turbulence level $\eta = \delta B_d/|\mathbf{B}_d|$ is larger close to the equatorial plane, in line with MHD simulations of the Nebula [7]. The turbulent field is defined on nested 3D grids, repeated periodically in space, using the method of [9]. We use isotropic turbulence with a Bohm spectrum, and with an outer scale equal to $L_{\text{max}} = 10^{18}$ cm $\approx 2 r_{\text{TS}}$ unless specified otherwise. The value of the minimum wavelength present in the turbulence is set to a fraction of the smallest gyroradius attained in the simulation, so that all particles experience resonant scattering. For technical reasons [8], we add weak turbulence in the upstream, but our results are not influenced by it. We inject electrons and positrons at the TS with their momenta directed along $+\hat{\mathbf{x}}$, and with an energy $E_{\text{inj},d} = 1$ TeV which is in the relevant range for the Crab Nebula. Defining z_{crit} as the height at which the gyroradius in $\mathbf{B}_d(z_{\text{crit}})$ of an injected particle is equal to z_{crit} , one has $z_{\text{crit}} = \sqrt{z_0 E_{\text{inj},d}/eB_{d,0}} \approx 5.8 \times 10^{14}$ cm $\sqrt{z_0/10^{17}}$ cm. The region where injected particles are efficiently accelerated is typically $|z| \lesssim$ several z_{crit} . We integrate the particle trajectories in the downstream and upstream rest frames where the electric fields vanish, performing a Lorentz transformation at each shock crossing. We take synchrotron losses into account. In the upstream, we consider two cases: We either assume that the stripes survive up to the TS and calculate the synchrotron losses in the full strength of the upstream magnetic field, or we calculate these losses in the phase-averaged field, $\mathbf{B}'_u(z)$, as may be expected, e.g., if the stripes were to be destroyed before reaching the TS.

3. Results

We show in Fig. 2 the trajectories of 4 electrons (left panel) and 4 positrons (right) injected at the TS ($x = 0$, solid black lines) at $|z| < 1.5 \times 10^{15}$ cm, and accelerated via the first-order Fermi process, in a simulation where $z_0 = 10^{17}$ cm and $\delta B_d = 30 \mu\text{G}$. The trajectories are plotted in the shock rest frame and projected onto the (x,z) plane. The dashed orange lines represent $z = \pm z_{\text{crit}}$. In the simulations, about 90 to 95% of injected particles are advected in the downstream without gaining energy. By comparing the two panels, one can see that the two signs of charge behave differently. For this pulsar polarity ($B_{d,0} > 0$), electrons are focused towards the equatorial plane (black dotted line), whereas positrons tend to be pushed away from it. This is due to drift motion on the shock surface: electrons entering the upstream at an altitude z_1 tend to come back in the downstream at z_2 such that $|z_2| < |z_1|$, whereas positrons tend to re-enter the downstream at

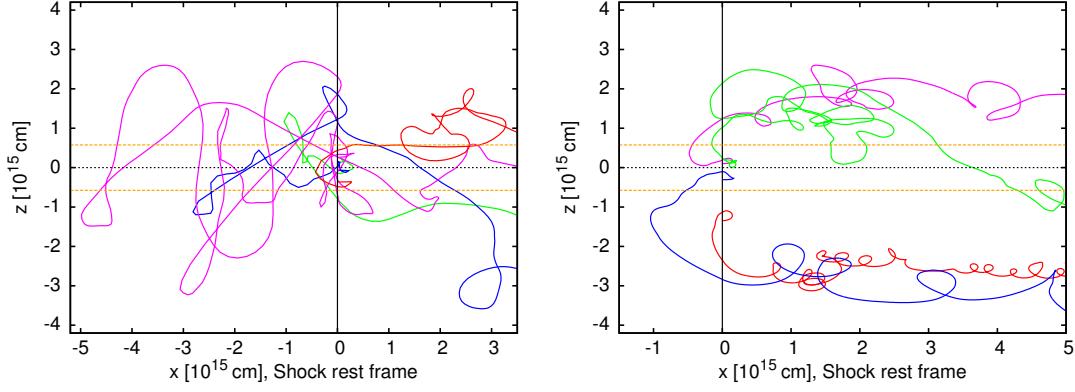


Figure 2: Left: Trajectories of electrons injected in the equatorial region of the TS. The upstream is on the left hand side of the shock ($x = 0$, solid black line). **Right:** Trajectories of positrons for the same parameters. See §3 for more details.

$|z_2| > |z_1|$. Since turbulence levels are larger at small $|z|$, electrons remain confined in the region which is the most favourable for diffusive shock acceleration. A number of them stay on “Speiser” orbits (e.g., the magenta trajectory in the left panel), and cross and re-cross the TS many times. In contrast, positrons are pushed away from this favourable region, and their acceleration quickly stops. Therefore, only electrons are accelerated to very high energies. For the opposite pulsar polarity ($B_{d,0} < 0$), the situation would be the opposite. The energy spectrum of the particles that are efficiently accelerated is a power-law $dN/dE \propto E^{\alpha_e}$, where α_e depends on the downstream turbulence level and lies in the range $\simeq -1.8$ to -2.4 . We plot in Fig. 3 (left panel) the values of α_e obtained in our simulations, versus $\eta_{\text{crit}} \equiv \delta B_d / |\mathbf{B}_d| |_{z=z_{\text{crit}}}$, for $z_0 = 10^{17}$ cm (solid red line) and $z_0 = 6 \times 10^{17}$ cm (black circles). We find that α_e is a function of η_{crit} and does not depend on z_0 . For low levels of turbulence $\eta_{\text{crit}} \approx 1 - 30$, the spectrum is harder than E^{-2} . It softens to $E^{-2.2}$ for larger turbulence levels, which corresponds to the slope that is required to explain the X-ray photon index of the Crab Nebula as measured by NuSTAR. At $\eta_{\text{crit}} < 1$, the spectrum also softens, but too few electrons are accelerated to explain the X-ray flux from the Nebula.

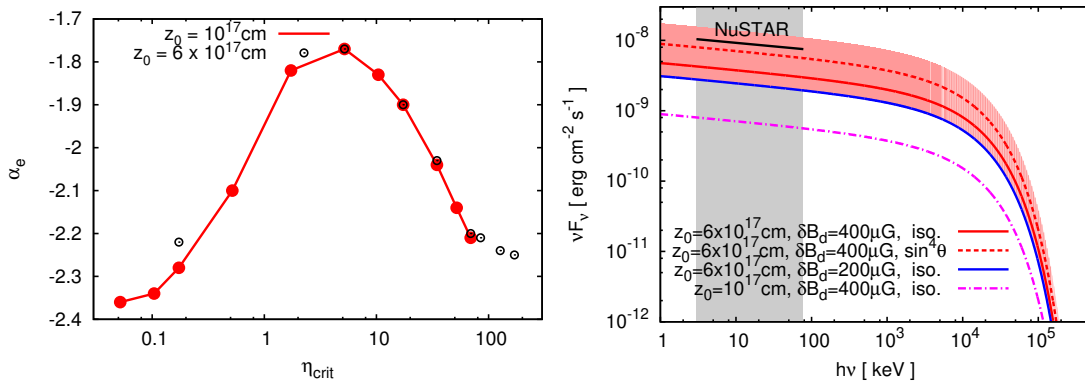


Figure 3: Left: Spectral index of the accelerated electrons, α_e , as a function of η_{crit} . **Right:** Predicted synchrotron spectra for the Crab Nebula versus NuSTAR measurements. See the text in §3 for explanations.

POS (ICRC2021) 913

Electrons accelerated at the TS are advected in the Nebula where they cool. We calculate the synchrotron spectrum from the cooled electrons and plot the results in Fig. 3 (right panel), for four sets of parameter values. See the key for the values of z_0 and δB_d , and for the isotropy (“iso.”) or anisotropy of the pulsar wind. We consider both isotropic and $\propto \sin^4 \theta$ winds, where θ denotes the colatitude. We use 2.0 kpc for the distance to the Crab pulsar. The effect of the uncertainty on this distance (± 0.5 kpc) for the two red lines is shown with the area shaded in red. The solid black line corresponds to the measurements from NuSTAR in the 3 – 78 keV band [2]. Our model can reproduce them for sufficiently large values of δB_d ($\geq 200 \mu\text{G}$) and z_0 . The magenta dashed-dotted line for $z_0 = 10^{17}$ cm (i.e., $\Theta \simeq 13^\circ$) and $\delta B_d = 400 \mu\text{G}$ is about an order magnitude below the measurements, but we obtain a larger X-ray flux for $z_0 = 6 \times 10^{17}$ cm (i.e., $\Theta \simeq 80^\circ$): the blue and red solid lines correspond to $\delta B_d = 200 \mu\text{G}$ and $\delta B_d = 400 \mu\text{G}$ for an isotropic wind. The red dashed line is for a $\propto \sin^4 \theta$ wind and $\delta B_d = 400 \mu\text{G}$. We can reproduce the data with these parameters. $|\mathbf{B}_d|(z) \propto |z|$ here, and the measurements would be reproduced with smaller values of Θ and δB_d , if one adopts a shallower dependence of $|\mathbf{B}_d|$ on z , such as in the profile in Komissarov’s 2013 model [17]. With this profile, we find that we can reproduce the data well with $\Theta = 60^\circ$ and $\delta B_d = 100 \mu\text{G}$ only.

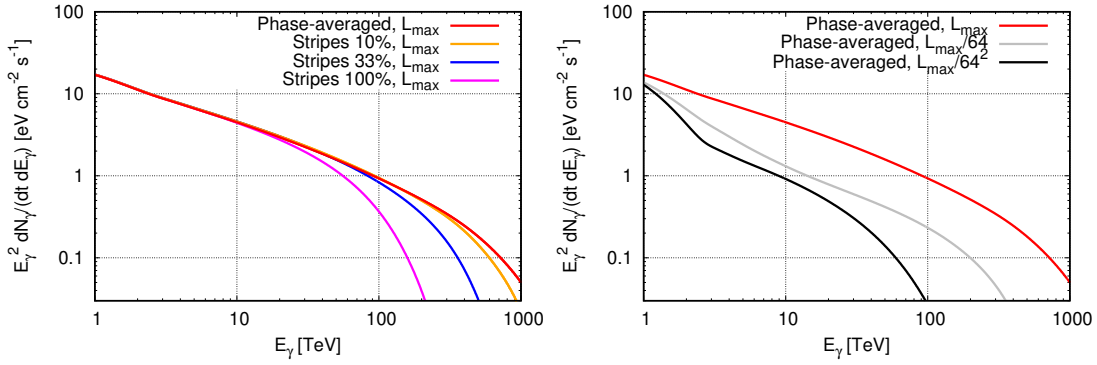


Figure 4: Gamma-ray spectrum of the Crab Nebula in our model, for $\Theta = 60^\circ$, $\delta B_d = 100 \mu\text{G}$, a $\propto \sin^4 \theta$ wind, and a “Komissarov profile” [17] for $|\mathbf{B}_d|$. The red line in both panels is for our reference case with an outer scale $L_{\text{max}} = 10^{18}$ cm $\approx 2 r_{\text{TS}}$ and where electrons cool in the phase-averaged field in the upstream. **Left:** The orange blue and magenta lines are for the case where the stripes survive up to the TS, and where electrons cool in 10%, 33%, and 100% of the full amplitude of the upstream magnetic field. **Right:** The grey and black lines are for outer scales equal to $L_{\text{max}}/64$ and $L_{\text{max}}/64^2$.

In Fig. 4, we present our calculations of the gamma-ray spectrum of the Crab Nebula with this “Komissarov profile”, and with a $\propto \sin^4 \theta$ wind. We also assume here that $\delta B_d = 100 \mu\text{G}$ and $\Theta = 60^\circ$. For the background photon fields, we use the values from the “constant B-field model” with $B = 125 \mu\text{G}$ of Ref. [18], and the distributions of the electron and photon densities in the Nebula that are provided in the “Appendix A” of [18].

The red curve in both panels shows the results for our reference case with an outer scale $L_{\text{max}} = 10^{18}$ cm $\approx 2 r_{\text{TS}}$, and where electrons cool in the phase-averaged field in the upstream. This curve fits well the existing observations of the Crab Nebula at energies $\lesssim 200$ TeV, and predicts that, for these parameters, the spectrum would continue unabated up to \sim PeV energies, and almost look like a pure power-law. Our predictions for the shape of the high-energy end ($\gtrsim 200$ TeV) of

the gamma-ray spectrum depends on unknown parameters of the Crab wind and Nebula however.

In the left panel, we show the dependence of the spectrum on the upstream magnetic field parameters. The magenta line shows the case where the stripes are assumed to survive up to the TS, and where the electrons cool in the full amplitude of the upstream magnetic field (assuming that $B_{d,0} = 1$ mG). In this case, the emission has a sharp turnover at lower energies, and the emission is strongly suppressed above ≈ 200 TeV. This is due to the fact that synchrotron cooling is more important when the stripes survive up to the TS and the magnetic field is therefore stronger close to the TS. The blue and orange lines show intermediate cases where the stripes partially survive up to the TS, but where the amplitude of the field in which the electrons cool in the upstream is only $1/3$ and $1/10$ of the full amplitude of this field.

In the right panel, we show how our results depend on the value of the outer scale of the turbulence, by reducing it. In this panel, we assume that the upstream magnetic field is the phase-averaged one for all 3 curves. The grey curve shows our calculations for an outer scale equal to $L_{\max}/64$ (where $L_{\max} = 10^{18}$ cm) and the black curve is for an outer scale equal to $L_{\max}/64^2$. One can clearly see that the maximum photon energy diminishes for decreasing values of the outer scale. This is due to the fact that very-high energy electrons are not strongly scattered by the turbulence any more once their gyroradius exceeds the outer scale of the turbulence. This, in turn, shuts down the acceleration process at high energies. The fact that the gamma-ray fluxes are lower for the grey and black curves at $\sim 1 - 10$ TeV is due to the fact that some of the electrons injected in the favourable equatorial region already have a gyroradius that is larger than the outer scale of the turbulence, which prevents them from being scattered into the upstream and accelerated.

4. Discussion

We find that the acceleration of X-ray emitting electrons occurs preferentially in the equatorial region of the TS. Interestingly, modeling of the high-energy emission from the Crab Nebula is compatible with these electrons being accelerated in, or close to, this region [10]. Shock-drift plays an important role, and ensures that the accelerated electrons remain in the equatorial region of the TS. For sufficiently large turbulence levels, the electron spectral index tends towards -2.2 , which is compatible with theoretical expectations [3]. For lower turbulence levels, the spectral index increases up to -1.8 . This may explain the hard photon index measured in the central regions of the Nebula by the Chandra X-ray Observatory [11], as turbulence levels may vary with time and position at the TS. We note that other effects, such as shock corrugation [12], may also play a role in the acceleration of X-ray emitting electrons, and that another acceleration mechanism may operate upon the electrons responsible for the radio to optical emission of the Nebula [10, 13]. The gamma-ray flares detected by AGILE and Fermi-LAT from the Crab Nebula require another acceleration mechanism too, such as inductive acceleration in the striped wind [14, 15]. The fact that each pulsar may accelerate preferentially either electrons or positrons to high energy, but not both, could have important implications for the interpretation of the positron fraction in cosmic-rays. Studies usually assume that pulsars accelerate electrons and positrons in equal numbers. Under this assumption, the fact that the AMS-02 positron fraction saturates well below 0.5 seems to rule out nearby pulsars as the main source of the high-energy electrons and positrons detected at Earth [16]. However, our above findings show that pulsars do remain viable candidates, as long as the local pulsar(s)

responsible for these fluxes accelerate preferentially electrons rather than positrons. Finally, our calculations also demonstrate that our model can reproduce well the observed gamma-ray spectrum of the Crab Nebula. The fact that the high-energy ends at $\gtrsim 100$ TeV of our predicted spectra depend on unknown parameters of the Crab pulsar wind and Nebula shows that near-future observations at \sim PeV energies, e.g. by LHAASO [19], will help to disentangle between different scenarios for the upstream magnetic field and downstream turbulence. This will allow for placing new constraints on unknown parameters of the Crab pulsar wind and Nebula.

5. Conclusions

We study particle acceleration at the TS of a striped pulsar wind. We find that either electrons or positrons are accelerated to very high energy, depending on the relative orientations of the magnetic and rotation axes of the pulsar. Drift motion on the shock surface keeps the accelerated particles close to the equatorial plane of the pulsar, allowing them to be accelerated by the first order Fermi process at the TS. Their energy spectrum is a power law, with index in the range -1.8 to -2.4 . Both the X-ray flux and photon index of the Crab Nebula, as measured by NuSTAR, can be reproduced for sufficiently large turbulence levels downstream of the shock. Moreover, our model also fits well existing observations in TeV gamma-rays of the Crab Nebula. Finally, our results strongly question the assumption often used in studies of the positron fraction that pulsars accelerate electrons and positrons to high energy in equal numbers. Taking this effect into account in future models would yield further interesting insights into the origin of the positron excess.

References

- [1] R. Bühler, R. Blandford, *The surprising Crab pulsar and its nebula: a review*, *Rep. Prog. Phys.* **77** (2014) 066901 [arXiv:1309.7046].
- [2] K. Madsen *et al.*, *Broadband X-ray Imaging and Spectroscopy of the Crab Nebula and Pulsar with NuSTAR*, *ApJ* **801** (2015) 66 [arXiv:1502.07765].
- [3] J. Bednarz, M. Ostrowski, *Energy Spectra of Cosmic Rays Accelerated at Ultrarelativistic Shock Waves*, *Phys. Rev. Lett.* **80** (1998) 3911 [astro-ph/9806181].
- [4] J. G. Kirk, A. W. Guthmann, Y. A. Gallant, A. Achterberg, *Particle Acceleration at Ultrarelativistic Shocks: An Eigenfunction Method*, *ApJ* **542** (2000) 235 [astro-ph/0005222].
- [5] M. C. Begelman, J. G. Kirk, *Shock-Drift Particle Acceleration in Superluminal Shocks: A Model for Hot Spots in Extragalactic Radio Sources*, *ApJ* **353** (1990) 66.
- [6] L. Sironi, A. Spitkovsky, *Particle Acceleration in Relativistic Magnetized Collisionless Pair Shocks: Dependence of Shock Acceleration on Magnetic Obliquity*, *ApJ* **698** (2009) 1523 [arXiv:0901.2578].
- [7] O. Porth, M. J. Vorster, M. Lyutikov, N. E. Engelbrecht, *Diffusion in pulsar wind nebulae: an investigation using magnetohydrodynamic and particle transport models*, *MNRAS* **460** (2016) 4135 [arXiv:1604.03352].

- [8] G. Giacinti, J. G Kirk, *Acceleration of X-Ray Emitting Electrons in the Crab Nebula*, *ApJ* **863** (2018) 18 [arXiv:1804.05056].
- [9] G. Giacinti, M. Kachelriess, D. V. Semikoz, G. Sigl, *Cosmic ray anisotropy as signature for the transition from galactic to extragalactic cosmic rays*, *JCAP* **7** (2012) 031 [arXiv:1112.5599].
- [10] B. Olmi, L. Del Zanna, E. Amato, N. Bucciantini, A. Mignone, *Multi-D magnetohydrodynamic modelling of pulsar wind nebulae: recent progress and open questions*, *J. Plasma Phys.* **82** (2016) 635820601 [arXiv:1610.07956].
- [11] K. Mori, D. N. Burrows, J. J. Hester *et al.*, *Spatial Variation of the X-Ray Spectrum of the Crab Nebula*, *ApJ* **609** (2004) 186 [astro-ph/0403287].
- [12] M. Lemoine, *A corrugated termination shock in pulsar wind nebulae?*, *J. Plasma Phys.* **82** (2016) 635820401 [arXiv:1607.01543].
- [13] M. Lyutikov, T. Temim, S. Komissarov, P. Slane, L. Sironi, L. Comisso, *Interpreting Crab Nebula's synchrotron spectrum: two acceleration mechanisms*, *MNRAS* **489** (2019) 2403 [arXiv:1811.01767].
- [14] J. G Kirk, G. Giacinti, *Inductive Spikes in the Crab Nebula: A Theory of Gamma-Ray Flares*, *Phys. Rev. Lett.* **119** (2017) 211101 [arXiv:1710.04493].
- [15] J. G Kirk, G. Giacinti, *Inductive Acceleration of Ions in Poynting-flux-dominated Outflows*, *ApJ* **884** (2019) 62 [arXiv:1908.06507].
- [16] S. Recchia, S. Gabici, F. A. Aharonian, J. Vink, *Local fading accelerator and the origin of TeV cosmic ray electrons*, *Phys. Rev. D* **99** (2019) 103022 [arXiv:1811.07551].
- [17] S. Komissarov, *Magnetic dissipation in the Crab nebula*, *MNRAS* **428** (2013) 2459 [arXiv:1207.3192].
- [18] M. Meyer, D. Horns, H.-S. Zechlin, *The Crab Nebula as a standard candle in very high-energy astrophysics*, *Astron. Astrophys.* **523** (2010) A2 [arXiv:1008.4524].
- [19] Z. Cao *et al.* [LHAASO Collaboration], *Ultrahigh-energy photons up to 1.4 petaelectronvolts from 12 γ -ray Galactic sources*, *Nature* **594** (2021) 33.